Brief communication: Mountain permafrost acts as an aquitard during an infiltration experiment monitored with ERT time-lapse measurements

Mirko Pavoni[1], Jacopo Boaga[1], Alberto Carrera[2], Giulia Zuecco[3], Luca Carturan[3] and Matteo Zumiani[4]

[1] Department of Geosciences, University of Padova, Padua, Italy
[2] Department of Agronomy, Food, Natural Resources, Animals and Environment, University of Padova, Legnaro (PD), Italy
[3] Department of Land, Environment, Agriculture and Forestry, University of Padova, Legnaro (PD), Italy
[4] Servizio Geologico, Provincia Autonoma di Trento, Italy

Correspondence to: Mirko Pavoni (mirko.pavoni@phd.unipd.it)

Abstract. Frozen layers within the subsurface of rock glaciers are generally assumed to act as aquicludes or aquitards. So far, this behavior has been mainly defined analyzing the geochemical characteristics of spring waters. In this work, for the first time, we experimentally confirmed this assumption by executing an infiltration test in a rock glacier of the Southern Alps, Italy. Time-lapse electrical tomography (ERT) technique was adopted to monitor the infiltration of 800 liters of salt-water spilled on the surface of the rock glacier. 24 hours ERT monitoring highlighted that the injected water was not able to infiltrate into the underlying frozen layer.

1 Introduction

In alpine regions, groundwater originating from moraines and rock glaciers is highly contributing to the streamflow (Wagner et al. 2016). Therefore, a key factor in the hydrological modeling of alpine catchments is the determination of the hydraulic properties of these landforms. The subsoil hydrodynamic of moraines, talus and hillslope aquifers is relatively well known, but the hydraulic behavior of rock glaciers and their impact on the hydrology of alpine catchments are relatively less defined (Pauritsch et al., 2017 and references therein). The hydrological and the geochemical monitoring of spring waters emerging downslope of active rock glaciers have been used to investigate runoff processes, the presence and role of frozen layers in alpine catchments (e.g., Krainer et al., 2007; Carturan et al., 2016). In active or ice-rich intact rock glaciers, continuous frozen layers are typically considered as aquicludes (Giardino et al., 1992). Krainer et al. (2007) separated a subsurface flow component, derived from snow-ice melting and rainwater, and a deeper and longer stored aquifer at the bottom of Reichenkar active rock glacier (Austrian Alps). Harrington et al. (2018) defined the inactive Helen Creek rock glacier (Alberta, Canada) as an unconfined aquifer, as the limited ground ice distribution is unlikely to act as a pure aquiclude. These investigations suggest that rock glaciers host complex and heterogeneous aquifers with a layered internal structure. Nevertheless, geochemical surveys have not the ability to accurately define the aquifer's structure (e.g., layers thickness, discontinuities, and lateral/vertical heterogeneities) if not integrated with geophysical surveys.

To verify and confirm the hydraulic behavior of the frozen layer, an infiltration experiment combined with electrical resistivity tomography (ERT) time-lapse measurements has been performed on the Sadole rock glacier (Southern Alps, Italy). Controlled irrigation experiments combined with ERT time-lapse measurements were successfully applied to study the vadose zone (Cassiani et al., 2006), or rarely in more challenging hillslope catchments (Cassiani et al., 2009). The Sadole rock glacier infiltration experiment represents the first attempt to adopt this monitoring technique to the mountain permafrost environment and, considering the promising results, can be used as reference to improve future tests and better characterize the hydraulic properties of the frozen subsoils.

2 Site description

The Sadole rock glacier is located in the Sadole Valley, in the Eastern part of the Trento Province (North-East Italy, Fig.1A). The rock glacier ranges between 1820 m a.s.l. and 2090 m a.s.l. and it is a complex periglacial landform that derives from the confluence of three different lobes (Fig.1B). This periglacial landform occupies the floor of two coalescent glacial cirques. Steep rock walls and sharp crests almost entirely bound these cirques, with the exception of the Sadole Pass that was likely a glacial transfluence saddle during the last glaciation. Slope deposits are found between the rock walls and the rock glacier rooting areas. These deposits have gravitational or mixed gravitational/debris-flow/avalanche origin and are predominantly active. From a geological point of view, the rock glacier is composed of magmatic rocks (riodacitic ignimbrites) that belong to the Athesian Volcanic Group, a late-Paleozoic (Permian) volcanic succession. The Sadole rock glacier has been classified as 'relict' in the inventory of Trento Province (Seppi et al., 2012), in agreement with the guidelines provided by the IPA Action Group (RGIK, 2022). Despite this, the general convex morphology and the low water temperature of its spring, ranging between 1.0 and 1.8°C in the ablation season, suggested that this rock glacier may preserve permafrost (Carturan et al., 2016 and references therein). In addition, ice outcrops have been observed in mid-summer two meters below the surface, in a pit dug during the 1st World War (green dot in Fig.1B). Therefore, several ERT transects (blue, violet, and brown lines in Fig.1B) have been collected in summer 2021 on the rock glacier, confirming the presence of a discontinuous frozen layer (see "deep" high resistivity areas in Figs.1D-E). Soil temperature sensors (red dots in Fig.1B) have been installed in different location of the rock glacier bodies. Finally, to evaluate the hydraulic behavior of the frozen layer, an infiltration experiment with ERT time-lapse measurements has been realized in middle June 2022. The ERT monitoring transect (red line in Fig.1C) has been located in the same area of the ERT surveys 2021, considering the maximum slope gradient, and specifically settled to detect how the injected water flows in the area where the frozen layer is present, and how it flows where the frozen layer ends.

3 Methods

3.1 Experiment principles

ERT surveys are performed to detect the electrical properties of the ground. The method can be used for monitoring time-dependent subsurface processes by repeating periodically the measurements using the same electrode array (Binley, 2015). This ERT data acquisition method is defined as "ERT time-lapse technique", and can be performed with controlled irrigation experiments (Cassiani et al., 2006; Cassiani et al., 2009). In these tests, a large amount of salt-water is released into the subsoil system, and the propagation of the injected water is investigated using the ERT time lapse survey. An ERT dataset is collected before the injection, at a time called time zero (t0). Subsequently, as the salt water propagates into the ground, new datasets are periodically acquired at defined time steps (t1, t2, …, tn). The changes of electrical properties in the subsoil, due to the injected water flow, are usually not clearly highlighted by comparing the individual inverted resistivity models. To enhance the variation from one-time step to the next, only the inverted model t0 is represented in terms of absolute resistivities, while the other time steps are plotted in terms of percentage variations of resistivity with respect to the t0 model (Binley, 2015).

3.2 Data acquisition

An ERT survey line of 72 electrodes, spaced 1.5 meters from each other (total length of 106.5 meters), has been centered with respect to the discontinuous frozen layer detected in ERT surveys 2021. The injection point has been placed in the middle of the array. The measurements have been performed with a Syscal Pro georesistivimeter (Iris Instruments), using a dipole-dipole configuration with different skips (1, 3, 5 and 7 - the skip represents the number of electrodes skipped to create a dipole), and a stacking range between 3 and 6 with 5% error threshold. The chosen configuration allowed to collect direct and reciprocals measurements and to estimate a reliable experimental error for the acquired datasets (Binley, 2015). The position, characteristics of the survey line, and the acquisition scheme, were defined to better highlights the flow of the injected water.

79   The chosen array in fact guarantees a good resolution in the shallower part of the subsurface thanks to the relatively short

80   spacing and low skips but at the same time a large penetration thanks to the total length of the array and higher skips.

81   Furthermore, a very large number of measuring points (2594) have been acquired to increase the possibility of detecting

82   resistivity variations in the subsurface due to water flow. Thanks to this high number of measured points, the characteristics

83   of the array, and the acquisition scheme, we tried to increase the reliability of our models even in areas where the sensitivity

84   is notoriously low (e.g. the bottom and the edges, Binley, 2015).

85   The ERT data quality in rock glacier environments is usually low due to the high contact resistances between electrodes and

86   boulders (Hauck & Kneisell, 2008). To partially overcome this problem, and increase the amount of injected current (Pavoni

87   et al., 2022), we inserted the electrodes between the boulders using sponges soaked with saltwater (Fig.2A). The sponges have

88   been wetted at the beginning of each measurement during the ERT time lapse survey, to reach (approximately) homogeneous

89   contact resistances for each collected dataset. Collecting measurements with different contact resistances could lead in fact to

90   changes in resistivity models not linked to the flow of the injected water.

91   The water for the experiment has been collected during the previous months, using ten 100-liter bins. The bins have been

92   placed on the Sadole rock glacier, in the point selected for the water injection, in the early spring, when snow cover was still

93   present (Fig.B). They were filled with snow and covered with nylon sheets pierced at their center to collect rainwater. This

94   way, in mid-June the bins were completely filled with a mixture of snowmelt and rainwater. Before the experiment, 3 kg of

95   NaCl were added to each bin to obtain a salt-water solution. After collecting the t0 dataset, 8 bins were emptied one after the

96   other, injecting 800 liters of salt-water into the subsurface system (Fig.2C). Four datasets have been acquired in the first hour,

97   followed by four datasets at hourly intervals, and a last dataset collected 24 hours after water injection. No rain or uncontrolled

98   water contribution happened during the experiment.

99   **3.3 Data processing**

100 The acquired datasets have been filtered removing quadrupoles with a stacking error higher than 5%, and a reciprocal error

101 higher than 20%. Only the common quadrupoles saved in all the filtered datasets have been used to perform the inversion

102 process of each dataset. The inversion modeling has been performed using the Python-based software ResIPy (Blanchy et al.,

103 2020), and an expected data error of 20% has been set according to the reciprocal check (Binley, 2015). Once a common

104 unstructured triangular mesh has been created, all the acquired datasets have been independently inverted. Only the t0 initial

105 model was plotted in terms of absolute electrical resistivity values (logarithmic scale), while the other models (t_n) obtained

106 with the ERT time-lapse survey were plotted as percentage variations in resistivity compared to the initial model t0. In order

107 to avoid emphasizing changes in the high resistivity zone, the percentage changes in resistivity were calculated using

108 logarithmic values. Since we defined an expected data error of 20%, tiny resistivity changes in the inverted tomograms are

109 considered not reliable to highlights the flow of the injected water. Therefore, in the time-lapse models, negative resistivity

110 variations lower than 10% are plotted in light gray color. Finally, to detect the frozen layer boundary in t0 model, we applied

111 the steepest gradient method (Chambers, 2012). This method, as suggested by forward modeling analysis, is the most reliable

112 to evaluate the thickness of the active layer (Herring et al., 2022).

113 **4 Results**

114 Figure 3A shows the resistivity section at t0. The high resistivities (ρ>30 kΩm) close to the surface are linked to the voids

115 among coarse debris and blocks, typical in rock glacier environments (Hauck and Kneisel, 2008). Below the top high resistivity

116 layer, lower values of resistivity (ρ<10 kΩm) are found and can be associated with a decrease in porosity and grain size of the

117 deposit, and a possible increase in humidity. At the south-west and north-east edges of the section this low resistivity layer

118 reaches the bottom of the model. On the other hand, in the central part of the model (30<x<70 m) a clear change is detected at

119 a depth of about 10 meters. Below this boundary, the resistivity rapidly increases (ρ>50 kΩm), highlighting the presence of a

120 frozen layer (Hauck and Kneisell, 2008). By applying the steepest gradient method in the vertical direction, we defined 55

121 kΩm as the upper boundary of the permafrost layer and the same value has been used to define its lateral termination.

122 In Fig. 3B high negative resistivity variations (>20%) show a quick vertical infiltration of the injected water up to a depth of

123 10 meters within the first 15 minutes after the injection. This wet area persisted below the injection point until the last survey

124 t10 (Fig.3M), even if it seems to slowly shrink from one data acquisition to the next. Negative resistivity variations in Figs.

125 3B-E indicate a downslope subsurface flow in the north-east direction above the identified frozen layer. Where the frozen layer

126 ends (x ≈ 70 m), the water clearly appears to be able to propagate deeper vertically. Concerning the upslope area (x<30 m),

127 the negative resistivity variations are found from the surface to the bottom of the section until t4 (Fig.3B-3F), highlighting a

128 main initial vertical infiltration of the injected water. In the following time steps the negative values develop mainly at few

129 meters of depth (Figs. 3F-3L), indicating a possible anomalous upslope subsurface flow (south-west direction). These negative

130 variations, upslope of the injection area, are still present after 24 hours (t10, Fig. 3M). but, at the same time, the water still

131 flows downslope in the north-east direction. On the other hand, inside the defined frozen layer negative resistivity variations

132 are practically null, suggesting that the injected water did not propagate through it.

133 **4 Discussion and conclusions**

134 High negative resistivity variations (>20%) observed for t1 close to the injection area indicate a rapid vertical infiltration of

135 the water due to the presence of boulders, fractures and coarse sediments with high vertical permeability. The large amount of

136 injected water has probably saturated this area, which has become the source of the subsurface flow. Although we do not have

137 any measurements of saturated hydraulic conductivity, we can speculate that hydraulic conductivities may be much higher (in

138 the order of 10^{-2} m/s) than the ones observed in shallow soil layers of young moraines, as found in the Swiss Alps by Maier et

139 al. (2021). Subsurface flow, moving downslope along the north-east direction, is likely originated at the boundaries between

140 large boulders and a finer sediment. This layer is in fact characterized by lower resistivities (in t0 ρ<10 kΩm) compared to the

141 shallower depths, and has likely lower permeability. Nevertheless, the presence of large boulders at various depths can lead to

142 funnel flow, and/or splitting of flow paths (Hartmann et al., 2020), which may have determined the infiltration of some injected

143 water upslope (south-west direction) the injection point. From t1 to t5 the negative resistivity variations suggest almost a

144 continuous subsurface flow in the north-east direction along the maximum slope gradient, whereas from t6 to t10 local negative

145 resistivity variations indicate the accumulation of injected water in areas where there is a likely local decrease in permeability,

146 and water may reside there for a longer period.

147 The experiment confirms the assumption that a continuous permafrost layer can act as an aquiclude (Giardino et al., 1992;

148 Krainer et al., 2007) or, if it discontinuos as in the Sadole rock glacier, as an aquitard (Harrington et al., 2018). Furthermore,

149 the survey confirms the reliability of the steepest gradient method to define the boundary of the frozen layer, and the high

150 heterogeneities (vertical and lateral) in mountain permafrost subsurface, as recently highlighted from continuous core drilling

151 by Phillips et al. (2023). Due to these high heterogeneities, a quantitative analysis regarding hydraulic conductivity just via

152 time-lapse ERT monitoring is very challenging. As highlighted by Mewes et al. (2017) with synthetic analysis and seasonal

153 field measurements, it is unrealistic to define the flow paths of water in mountain permafrost subsurface just via resistivity

154 changes in tomograms. Moreover, the sampling step of the ERT datasets is forced by the necessary acquisition time and may

155 be too large, especially in the initial phases. In our case, due to logistical problems (adverse weather), it was not possible to

156 extend the survey measurements for the time necessary to return completely to the pre-injection conditions.

157 Future development of the current work is to perform the experiment in an active rock glacier during late summer, in order to

158 test the flow paths with a fully developed active layer, collecting datasets with a shorter sampling step and for a longer period,

159 until the subsurface system returns completely to the pre-injection conditions. In this way, a possible estimation of the active

160 layer average hydraulic conductivity could be achieved.

161
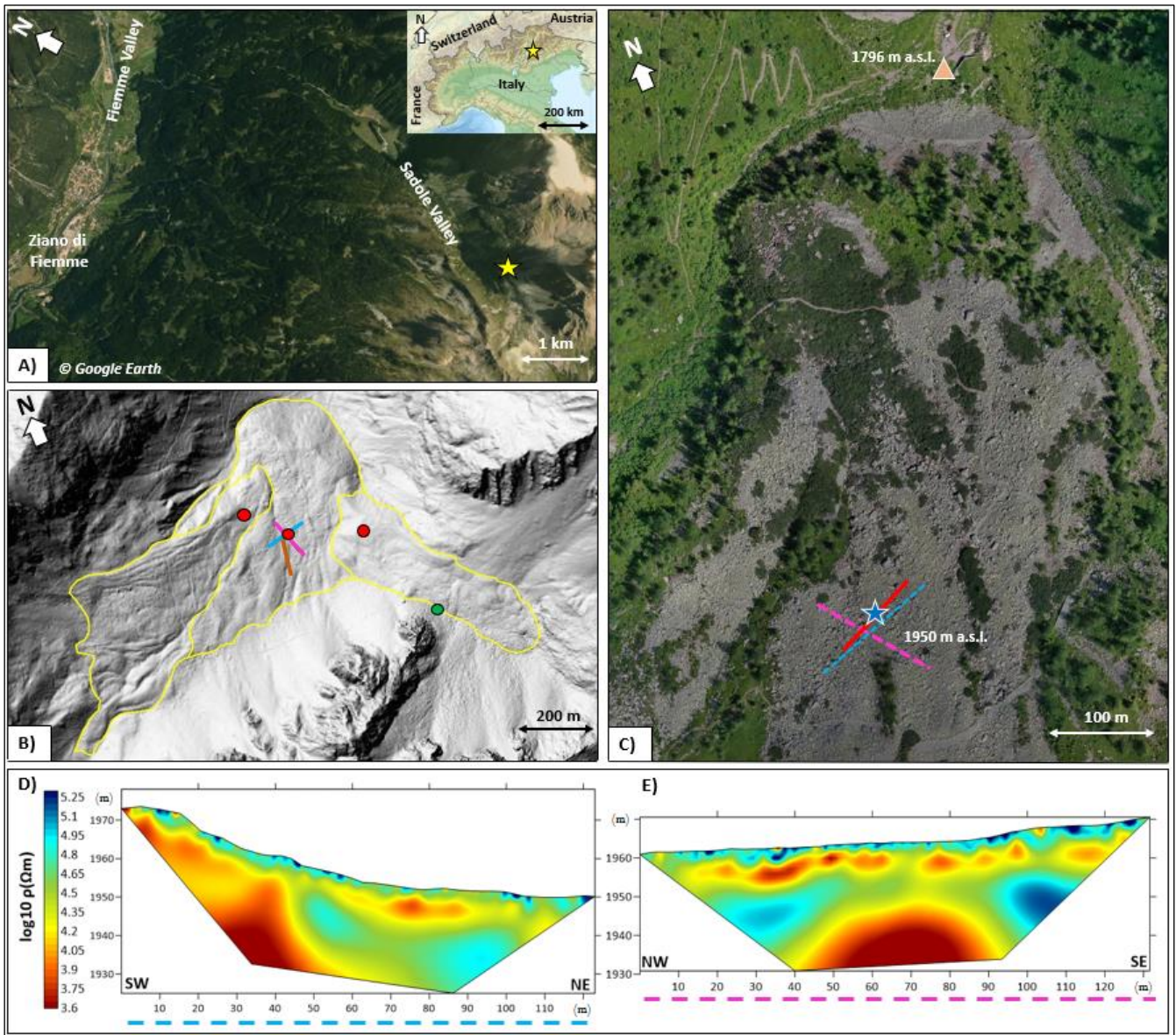
Figure 1: A) Geographic location of the Sadole rock glacier (yellow star), adapted from © Google Earth Pro and Italian Physical Map produced by The University of Texas at Austin; **B)** hillshaded LiDAR DEM (modified from WebGIS PAT – Provincia Autonoma di Trento) showing the three different units that compose the Sadole rock glacier (yellow lines). Blue, violet, and brown lines represent ERT surveys performed in summer 2021, red circles defines the position of soil temperature sensors, and green circle is the location of the Austrian well (1st World War); **C)** Orthophoto (Commissione Glaciologica SAT, 2022) showing the ERT transect (red line) used for the infiltration experiment, the salt water injection point (blue star – 1950 m a.s.l.), and the location of the rock glacier spring (brownish triangle – 1796 m a.s.l.). Blue and violet dashed lines represent ERT surveys performed in 2021 and showed in larger scale in Fig.1B. **D)** Inverted resistivity section of the blue survey line performed in summer 2021. **E)** Inverted resistivity section of the violet survey line performed in summer 2021.
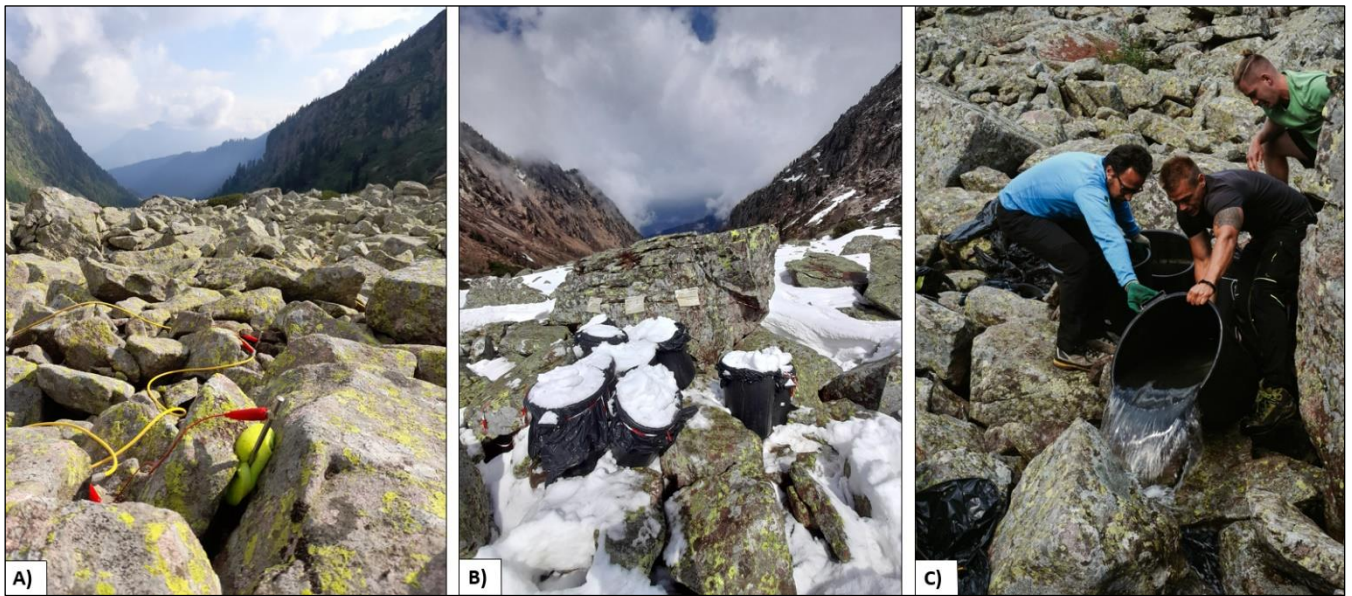
Figure 2: A) Electrodes inserted between the boulders using sponges soaked with saltwater to improve the contact resistances of the ERT surveys; B) 10 bins placed at the selected injection point in early spring 2022, filled with snow and covered with nylon sheets pierced at their center to collect rainwater; C) injection of 800 liters of salt water into the subsoil system.
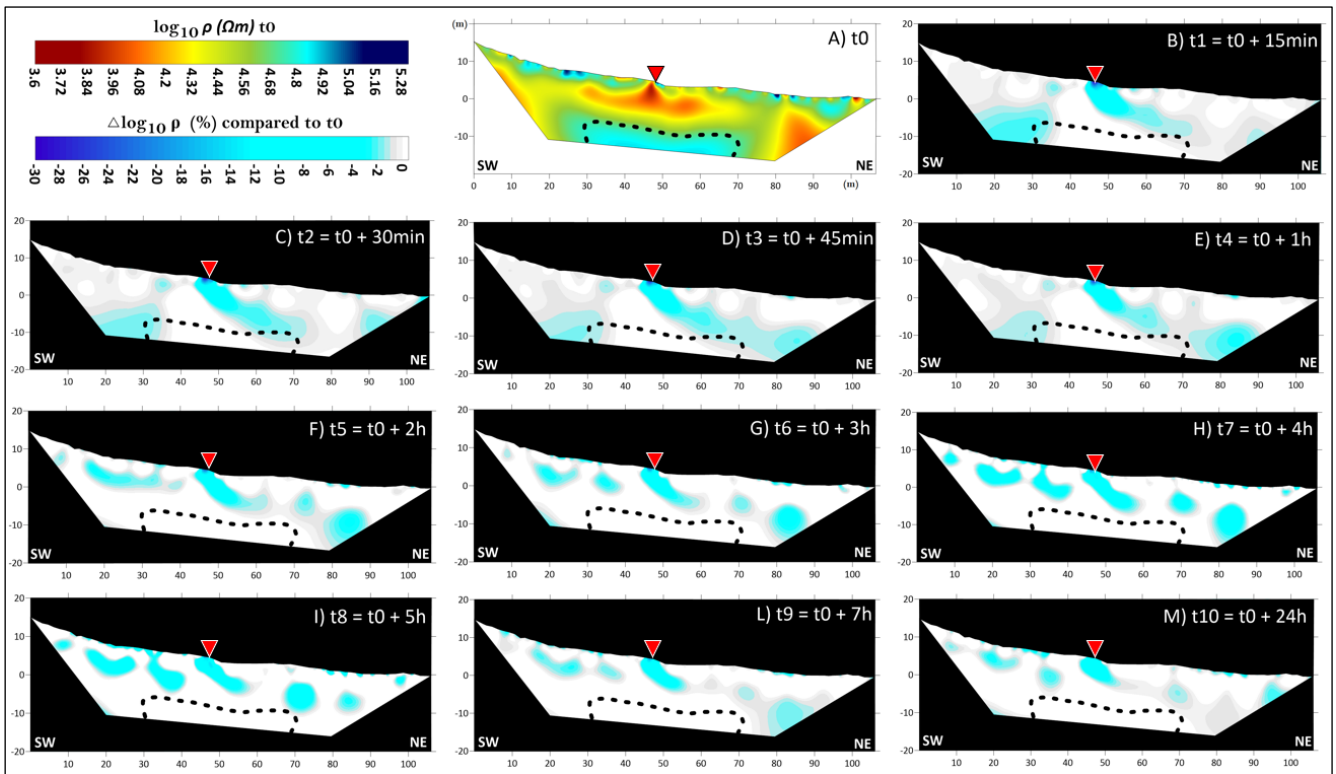
Figure 3: A) Inverted resistivity section calculated from the t0 dataset. Inverted resistivity variations (%), compared to t0 model, calculated using the logarithmic values for B) t1 dataset (t0 + 15 minutes), C) t2 dataset (t0 + 30 minutes), D) t3 dataset (t0 + 45 minutes), E) t4 dataset (t0 + 1 hour), F) t5 dataset (t0 + 2 hours), G) t6 dataset (t0 + 3 hours), H) t7 dataset (t0 + 4 hours), I) t8 dataset (t0 + 5 hours), L) t9 dataset (t0 + 7 hours), and M) t10 dataset (t0 +24 hours). The black dashed line represents the boundary of the frozen layer defined applying the steepest gradient method to the inverted resistivity model t0. Red triangles represent the injection point of 800 liters of salt-water.

186 *Author contributing*. MP, JB, AC and MZ have been involved in data acquisition; MP performed the data processing; LC

187 realized the geological framework; GZ carried out the interpretation of the results; all authors contributed to the writing and

188 editing of the manuscript.

189 *Acknowledgements*. Authors thanks Tommaso and Barbara, managers of "Il rifugio Baita Monte Cauriol", for logistical

190 support; the "Magnifica Comunità di Val di Fiemme" and "Comune di Ziano" for authorizing the investigations; and the

191 "Servizio Geologico della Provincia Autonoma di Trento" for the support.

192 *Data Availability Statement*. The datasets used to obtain the results presented in this work are avaible at the open source

193 repository: https://zenodo.org/badge/latestdoi/541527187 (DOI: 10.5281/zenodo.7113054).

194 **References**

195 Binley, A: Tools and Techniques: Electrical Methods. In: Gerald Schubert (editor-in chief), Treatise on Geophysics, 2nd
196 edition, Vol 11. Oxford: Elsevier; p. 233-259, https://doi.org/10.1016/B978-0-444-53802-4.00192-5, 2015.

197 Blanchy, G., Saneiyan, S., Boyd, J., McLachlan, P., and Binley, A.: ResIPy, an intuitive open source software for complex
198 geoelectrical inversion/modeling. Computers & Geosciences, 137, 104423, https://doi.org/10.1016/j.cageo.2020.104423,
199 2020.

200 Carturan L., G. Zuecco, R. Seppi, T. Zanoner, M. Borga, A. Carton, and D. Dalla Fontana: Catchment scale permafrost
201 mapping using spring water characteristics. Permafrost and Periglacial Processes, 27, 253-270,
202 https://doi.org/10.1002/ppp.1875, 2016.

203 Cassiani G., Binley A.M., and Ferre T.P.A.: Unsaturated zone processes. In: Applied Hydrogeophysics (eds H. Vereecken, A.
204 Binley, G. Cassiani, A. Revil and K. Titov), pp. 75–116, Springer Verlag, https://doi.org /10.1007/978-1-4020-4912-5_4, 2016.

205 Cassiani, G., Godio, A., Stocco, S., Villa, A., Deiana, R., Frattini, P., and Rossi, M.: Monitoring the hydrologic behavior of a
206 mountain slope via time-lapse electrical resistivity tomography. Near Surface Geophysics, 7(5-6), 475-486,
207 https://doi.org/10.3997/1873-0604.2009013, 2009.

208 Chambers, J. E.: Bedrock detection beneath river terrace deposits using three-dimensional electrical resistivity tomography.
209 602 Geomorphology, 177–178, 17–25, https://doi.org/10.1016/j.geomorph.2012.03.034, 2012.

210 Giardino, J. R., Vitek, J. D., and Demorett, J. L.: A model of water movement in rock glaciers and associated water
211 characteristics. In Periglacial Geomorphology: Proceedings of the 22nd Annual Binghampton Symposium in Geomorphology,
212 pp. 159–184, 1992.

213 Harrington, J. S., Mozil, A., Hayashi, M., and Bentley, L. R.: Groundwater flow and storage processes in an inactive rock
214 glacier. Hydrological Processes, 32(20), 3070-3088, https://doi.org/10.1002/hyp.13248, 2018.

215 Hartmann A., Semenova E., Weiler M., and Blume T.: Field observations of soil hydrological flow path evolution over 10
216 millennia. Hydrology and Earth System Sciences, 24, 3271–3288, https://doi.org/10.5194/hess-24-3271-2020, 2020.

217 Hauck, C., and Kneisel, C.: Applied Geophysics in Periglacial Environments, Cambridge University Press, 2008.

218 Herring, T., and Lewkowicz, A. G.: A systematic evaluation of electrical resistivity tomography for permafrost interface
219 detection using forward modeling. Permafrost and Periglacial Processes, https://doi.org/10.1002/ppp.2141, 2022.

220 Krainer K., Mostler W., and Spötl C.: Discharge from active rock glaciers, Austrian Alps: a stable isotope approach. Austrian
221 Journal of Earth Sciences, 100, 102-112, 2007.

222 Maier F., van Meerveld I., Weiler M. Long-term changes in runoff generation mechanisms for two proglacial areas in the
223 Swiss Alps II: Subsurface flow. Water Resources Research, 57, e2021WR030223. DOI:10.1029/2021WR030223, 2021.

224 Mewes, B., Hilbich, C., Delaloye, R., and Hauck, C.: Resolution capacity of geophysical monitoring regarding permafrost
225 degradation induced by hydrological processes, The Cryosphere, 11, 2957–2974, https://doi.org/10.5194/tc-11-2957-2017,
226 2017.

227 Pauritsch, M., Wagner, T., Winkler, G., and Birk, S.: Investigating groundwater flow components in an Alpine relict rock
228 glacier (Austria) using a numerical model. Hydrogeology Journal, 25(2), 371-383, 2017.

229 Pavoni, M., Carrera, A., and Boaga, J.: Improving the galvanic contact resistance for geoelectrical measurements in debris
230 areas: a case study. Near Surface Geophysics, https://doi.org/10.1002/nsg.12192, 2022.

231 Phillips, M., Buchli, C., Weber, S., Boaga, J., Pavoni, M., and Bast, A.: Brief communication: Combining borehole
232 temperature, borehole piezometer and cross-borehole electrical resistivity tomography measurements to investigate seasonal
233 changes in ice-rich mountain permafrost, The Cryosphere, 17, 753–760, https://doi.org/10.5194/tc-17-753-2023, 2023.

234 RGIK (2022). Towards standard guidelines for inventorying rock glaciers: baseline concepts (version 4.2.2). IPA Action Group
235 Rock glacier inventories and kinematics, 13 pp.

236 Seppi, R., Carton, A., Zumiani, M., Dall' Amico, M., Zampedri, G. and Rigon, R.: Inventory, distribution and topographic
237 features of rock glaciers in the southern region of the Eastern Italian Alps (Trentino). Geogr. Fis. Dinam. Quat. 35 (2012), 185-
238 197, https://doi.org/10.4461/GFDQ.2012.35.17, 2012.

239 Wagner T., Pauritsch M., and Winkler G.: Impact of relict rock glaciers on spring and stream flow of alpine watersheds:
240 examples of the Niedere Tauern Range, Eastern Alps (Austria). Aust J Earth Sci 109, https://doi.org/10.17738/ajes.2016.0006,
241 2016.